NEW ATOM-PROBE TOMOGRAPHY DATA AND IMPROVED TECHNIQUES FOR METEORITIC NANODIAMOND ANALYSIS

J. B. Lewis[1,3], D. Isheim[4], C. Floss[1,3], T. L. Daulton[2,3], D. N. Seidman[4]. [1]Laboratory for Space Sciences, [2]Center for Materials Innovation, [3]Physics Dept., Washington University, St. Louis, MO. Email: jblewis@go.wustl.edu. [4]Center for Atom-Probe Tomography, Dept. of Materials Science and Engineering, Northwestern University, Evanston, IL.

Introduction: Studies of meteoritic nanodiamonds have proceeded along a unique path compared to other presolar grains. Nanodiamonds were the first phase isolated associated with isotopic anomalies [1] and yet, more than two decades later, their origin remains unclear. Limitations in sensitivity and spatial resolution have permitted only bulk measurements of millions of ~3 nm [2] nanodiamonds in aggregate. These measurements exhibit isotopic anomalies in noble gas and trace elements [1, 3, 4, 5], but major and minor element isotopic ratios (e.g., C and N) are consistent with the solar values [6,7]. There are many formation theories for nanodiamonds, but without measuring the isotopic ratios of individual nanodiamond grains it is impossible to determine whether sub-populations of isotopically anomalous nanodiamonds are present and to constrain their origins more definitively. Recent research [8] has demonstrated that atom-probe tomography (APT) is a promising technique for the isotopic analyses of nanodiamonds on the sub-nanometer to nanometer scale. Herein we present C isotope measurements from 11 new Allende nanodiamond (ND) samples, each estimated to contain between 1–100 meteoritic NDs. We also present measurements from three new detonation nanodiamond (DND) standard samples, and discuss new processing, bias correction, and analysis techniques.

Experimental: Measurements are made with a Cameca LEAP 4000X Si atom-probe tomograph [8, 9]. In APT ([10] and references therein) we employ a high electric-field bias accompanied by nanosecond laser pulsing to field-evaporate one atom at a time from a microtip with a 20–100 nm radius needle-shaped sample and project them onto a microchannel plate detector. Sample microtips are composed of NDs sandwiched between sputter-deposited Pt [8] (Fig. 1). APT combines point projection field-ion microscopy and time-of-flight mass spectrometry and permits reconstruction of the 3-D locations and mass-to-charge-state ratios of atoms and molecules originating in a microtip.

Processing Improvements: We have tailored our multilayer liftout and microtip mounting sample preparation technique as well as APT experimental parameters, to improve microtip lifetime and stability in the atom probe [e.g., 8]. Hydride formation is a concern because, while the mass resolving power in APT is sufficient to distinguish ^{12}C and ^{13}C in all common charge states, it will not distinguish $^{13}C^+$ from $(^{12}CH)^+$. To evaluate hydride formation in our data, we employ correlated ion-detection event analysis, known as multiple-hit analysis [11], which highlights ion species that tend to field-evaporate during the same laser pulse (Fig. 2). We detected few correlated $(^{12}CH)^+$ events compared to total events at 13 Da, suggesting only low levels of hydride formation in our data, but further, quantitative analysis of microtips and subvolumes is warranted. The detection efficiency in APT, which is about 50% plus of the atoms in a sample, is another concern. For a 3 nm ND and a $^{12}C/^{13}C$ isotopic ratio of ~90/1, we anticipate detection of at most 11 ^{13}C atoms. Thus, it is essential to maximize detection efficiency to make statistically significant measurements of the $^{12}C/^{13}C$ isotopic ratio. Multiple-hit analyses can be used to estimate the probability of a pair of ions being lost due to the detector's deadtime: ^{12}C and ^{13}C loss at the detector appears to be minimal. A final concern is that it is not straightforward to reconstruct the original position of ions based on its detected location. For example, diamond is preferentially magnified in 3-D reconstructions compared to the Pt matrix, because it evaporates at a higher value of the electric field. In future work we will employ transmission electron mi-

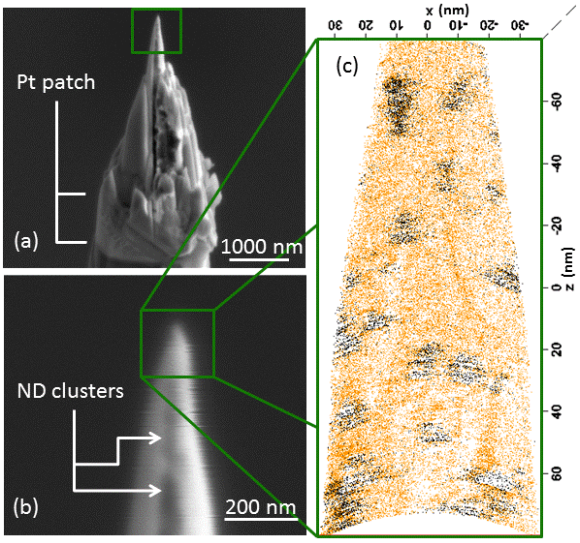

Fig. 1. (a) A microtip attached to a Si micropost by a Pt patch. (b) The same tip at higher magnification, displaying dark ND clusters in the deposition layer. (c) Cross-section of reconstructed APT data exhibiting individual NDs (black dots are C atoms) in a Pt matrix (orange dots).

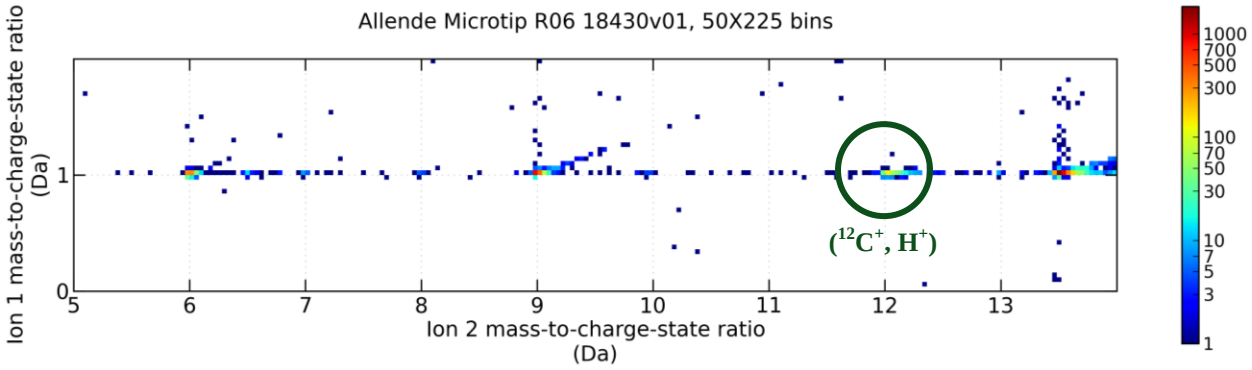

Fig. 2. 2D APT mass histogram plotting the mass-to-charge-state ratios of pairs of ions (double events) detected during the same laser pulse cycle. Hot spots correspond to ion species that tend to co-evaporate. Horizontal and vertical streaks represent a tendency for one ion in a pair to evaporate normally while the other evaporates shortly after the peak of the pulse. Diagonal lines represent pairs where both ions experience delayed evaporation. Visible in this range is the co-evaporation, or lack thereof, of H (1 Da) with C ions (6, 6.5, 12, 13 Da) and Al ions (9, 13.5 Da).

croscopy (TEM) analyses to address this issue by measuring the original dimensions and shape of diamonds prior to APT analyses.

Discussion: The new DND standard ratios are in better agreement with each other than are the ratios in [8] (Fig. 3). The new data were taken with more standardized run conditions and after atom probe hardware upgrades. In particular the new DND $^{12}C^{++}/^{13}C^{++}$ ratios, which should be unaffected by CH hydrides, exhibit the least scatter. All the measured standard ratios are lower than the terrestrial value of ~89, implying a consistent instrumental bias that affects all our data. Another bias is implied by the fact that the Allende

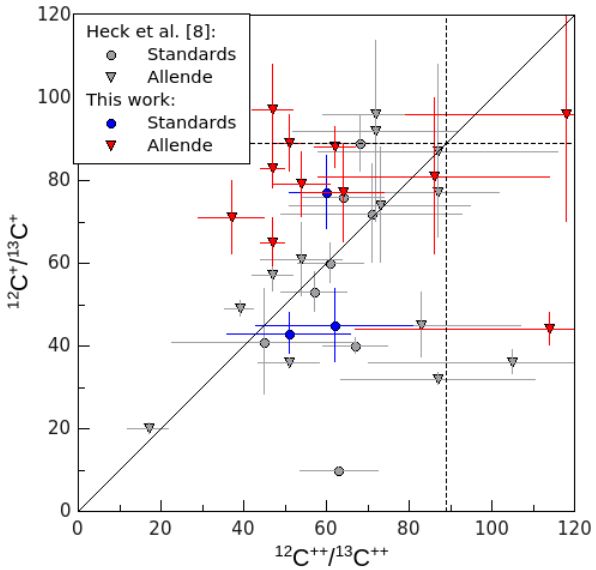

Fig. 3. Graphical summary of $^{12}C/^{13}C$ isotopic ratios determined by APT. Each data point represents the ratios of counts from an individual microtip. Errors are one σ, based on counting statistics. Dashed lines mark the terrestrial $^{12}C/^{13}C$ ratio of ~89. The solid diagonal line indicates where equal ratios for singly- and doubly-charged C ions lie.

$^{12}C^{+}/^{13}C^{+}$ ratios are generally larger than the corresponding $^{12}C^{++}/^{12}C^{++}$ ratios. This is inconsistent with hydride interference on $^{13}C^{+}$, which would *decrease* the $^{12}C^{+}/^{13}C^{+}$ ratios. We note that the NDs are mixed with an amorphous C phase [12]. If some of the "nanodiamonds" detected in the Allende data are actually a different phase of C, they may co-evaporate more or less readily with H than the DNDs, so hydride interference, if it occurs, may not have the same effect on all of the Allende data as it does on the standards. Finally, Allende ratios that are significantly larger or smaller than the DND ratios could be due to inherent isotopic anomalies in the meteoritic NDs. While our new standard data set is not yet large enough to be statistically significant, the new Allende ratios appear to be larger than the standard ratios.

Outlook: We will continue to refine our standard measurements and reproducibility using APT analyses of DNDs and NanoSIMS [13] analysis of meteoritic NDs and standards such as DNDs, chemical vapor deposition nanodiamonds, ^{12}C–^{13}C multilayers (Isheim et al., 2014, unpublished), and graphite. TEM will be employed to assess 3-D reconstruction errors, such as preferential magnification.

References: [1] Lewis R. S. et al. (1987) *Nature*, *326*, 160–162. [2] Daulton T. L. et al. (2006) *GCA*, *60*, 4853–4872. [3] Richter S. et al. (1998) *Nature*, *391*, 261–263. [4] Maas R. et al. (2001) *MAPS*, *36*, 849–858 [5] Lewis R. S. et al. (1991) *LPS XXII*, 807–808. [6] Russell S. R. et al. (1996), *MAPS*, *31*, 343–355. [7] Marty B. et al. (2011) *Science*, *332*, 1533–1536. [8] Heck P. R. et al. (2014) *MAPS*, in press. [9] Isheim D. et al. (2013) *Microsc. Microanal.*, *19* (Suppl 2), CD974–CD975. [10] Gault B. et al. (2012) *Atom Probe Microscopy*, Springer. [11] Saxey D. W. (2011) *Ultramicroscopy*, *111*, 473–479. [12] Stroud R. M. et al. (2011) *ApJL*, *738*, L27–L31. [13] Lewis J. B. et al. (2013) *LPS XLIV*, #2506.

This work is supported by NASA grant NNX13AF53G (C.F.)